Climatology and changes in tropical oceanic rainfall characteristics inferred from Tropical Rainfall Measuring Mission (TRMM) data (1998–2009)

K.-M. Lau[1] and H.-T. Wu[2]

Received 18 February 2011; revised 12 May 2011; accepted 13 June 2011; published 14 September 2011.

[1] This study investigates the climatological and changing characteristics of tropical rain and cloud systems in relation to sea surface temperature (SST) changes using Tropical Rainfall Measuring Mission (TRMM) data (1998–2009). Rainfall and cloud characteristics are determined from probability distribution functions (pdf), derived from daily TRMM Microwave Imager (TMI) and Precipitation Radar (PR) surface rain, Visible and Infrared Scanner (VIRS) brightness temperature (T_b), and PR echo top height (H_{ET}). Results show that the top 10% heavy rain is associated with cold cloud tops (T_b < 220 K) and elevated echo top heights (H_{ET} > 6 km), associated with ice phase rain in the Intertropical Convergence Zone and monsoon regions. The bottom 5% light rain occurs most frequently in the subtropics and also in the warm pool regions with low cloud top (T_b > 273 K) and H_{ET} ~ 1–4 km. Intermediate rain (25th to 75th percentile) is contributed by a wide range of middle clouds and mixed-phase rain centered at T_b ~ 230–260 K and H_{ET} ~ 4–6 km within the warm pool. The relationships between rainfall and SST depend strongly on rain types. We find that a warmer tropical ocean favors a large increase in annual heavy rain accumulation, a mild reduction in light to moderate rain, and a slight increase in extremely light rain. The annual accumulation of extreme heavy rain increases approximately 80%–90% for every degree rise in SST, much higher than that expected from the Clausius-Clapeyron equation for global water balance. This is possibly because heavy rain is only a component of the tropical water cycle and is strongly associated with ice phase processes and convective dynamics feedback.

Citation: Lau, K.-M., and H.-T. Wu (2011), Climatology and changes in tropical oceanic rainfall characteristics inferred from Tropical Rainfall Measuring Mission (TRMM) data (1998–2009), *J. Geophys. Res.*, *116*, D17111, doi:10.1029/2011JD015827.

1. Introduction

[2] It remains a subject of debate whether long-term trends in global precipitation can be detected with current global rainfall data sets, and whether or not trends in precipitation should follow the Clausius-Clapeyron relation, i.e., approximately 7% increase per degree rise in temperature [*Intergovernmental Panel on Climate Change*, 2007]. *Wentz et al.* [2007] found a global precipitation trend of +6% °C^{-1} from satellite data for the period 1988–2006. *Adler et al.* [2008] found, using similar data but for a different period (1979–2006), a much smaller value of +2.3% °C^{-1}, which is more consistent with model results [*Allen and Ingram*, 2002; *Held and Soden*, 2006]. Over the tropics, the trends tend to be more sensitive to sea surface temperature (SST) changes, estimated to be in the range of +5%–11% °C^{-1} (land and ocean) [*Gu et al.*, 2007; *Adler et al.*, 2008]. Others have found higher sensitivity of approximately +13% °C^{-1} for tropical wet regions and lower and negative sensitivity of about −2.3% °C^{-1} for tropical dry regions [*Allan et al.*, 2010]. The global and tropical total rainfall trends tend to be small and have large uncertainties. However, more significant changes in rainfall characteristics, in the form of increased frequency and intensity of extreme events such as droughts, floods, and tropical cyclone activities attributable to climate change have been found [*Trenberth et al.*, 2003; *Easterling et al.*, 2000]. There is now growing evidence of long-term (multidecadal) trends in rainfall distribution, with increasing frequency of extreme precipitation events in tropical and subtropical regions [*Shepherd et al.*, 2007; *Lau and Wu*, 2003, 2007; *Lau et al.*, 2008; *Allan and Soden*, 2008]. So far most of the aforementioned studies on extremes have used either station data over land or long-term monthly satellite-derived rainfall from operational satellites. These data are less than optimal in the sense of limited spatial coverage, temporal homogeneity, and compatibility with ancillary data which are needed to determine changes in rainfall characteristics and extremes.

[3] The Tropical Rainfall Measuring Mission (TRMM) has now accumulated more than 12 years of state-of-the-art

[1]Laboratory for Atmospheres, NASA Goddard Space Flight Center, Greenbelt, Maryland, USA.
[2]Science Systems and Applications, Inc., Lanham, Maryland, USA.

Copyright 2011 by the American Geophysical Union.
0148-0227/11/2011JD015827

rainfall products with higher spatial (0.25° × 0.25° latitude by longitude) and temporal (daily and 3-hourly) resolution, including rain rates, rain types, structure, latent heating profiles and related water vapor and cloud properties. These data products have offered an unprecedented opportunity for research for a diverse range of topics related to precipitation and cloud physics, regional and global water cycles, weather and climate. The planned Global Precipitation Measurement (GPM) mission will further expand the data sets to a global domain with improved sampling and detection for midlatitude rain systems, including solid precipitation.

[4] Because 12 years of data is still woefully inadequate for detecting long-term changes in total rainfall, this study represents a best effort approach to use a variety of TRMM products to shed light on the climatology and possible changes in rainfall characteristics as a function of sea surface temperature (SST). The objectives of this study are modest: (1) to document and elucidate the basic physical underpinnings of the relationships between rainfall characteristics and SST using TRMM data and (2) to serve as a benchmark for future extended analyses into the GPM timeframe. The organization of this paper is as follows. Section 2 describes the data products and analysis procedure. Section 3 presents a comparison of the rainfall climatological characteristics derived from the two TRMM instruments, the Tropical Microwave Imager (TMI) and the Precipitation Radar (PR). Section 4 describes cloud characteristics associated with different rain types. Section 5 discusses the possible changes in rainfall characteristics, as a function of tropical mean SST for different rain types. Concluding remarks are presented in section 6.

2. Data and Analysis Procedure

[5] To ensure the robustness of the results, we carry out identical analyses on two independent TRMM rainfall (Version 6) products, TMI (2A12) and PR daily surface rain rate (2A25), for the period 1998–2009. Details on the TRMM sensors and data algorithms are given by *Kummerow et al.* [1998]. The Hadley Center monthly data is used for the sea surface temperature (SST) analysis [*Rayner et al.*, 2003]. In addition, we use PR echo top height (TRMM product 2A23, H_{ET}) and Visible and Infrared Scanner (VIRS) channel-4 brightness temperature (TRMM product 1B01, T_b) to define the cloud characteristics associated with different rain types. For this work, we preprocess all TRMM products on a daily, common 0.5° × 0.5° grid box average. The rain rate and T_b averages are unconditional means and the H_{ET} average is conditional mean. To account for the sampling biases due to TRMM's orbital geometry and sensors' swath widths, the number of valid daily observations at each grid box in each year is calculated and used as the weighting function to estimate the yearly statistics of that grid box [*Lin et al.*, 2002]. The latitudinal dependence of sampling frequencies has also been taken into account in calculating the tropical mean statistics.

[6] A comparison of the preboost and postboost data indicates a systematic bias due to the effect of TRMM orbit boost in August 2001. To minimize the bias due to the orbit boost, we develop and apply a rain rate–dependent adjustment to the TMI and PR data. The adjustment is based on computation of a bias function derived from the difference in the rainfall probability distribution function sampled from equal length periods before and after the boost. To minimize the effect of SST, we avoid using years with moderate to strong warm or cold events (1998, 1999, 2000, 2002, 2003, 2007, 2008, 2009). From the remainder of the years, we examine the SST anomaly pattern and magnitude and find that the years 2001 and 2006 have very similar SST anomaly patterns, with small amplitude deviations from climatology. Henceforth, we select the period January through July between year 2001 and the same calendar months for year 2006 for calculation of the bias function. The same months are used to minimize the effect of the seasonal cycle. The adjustment in the form of a multiplicative factor for binned rain rate was applied to the preboost data because the postboost period is much longer than the preboost period. For TMI, the most obvious effect of the orbit boost is about 2%–4% decrease in light to moderate rain and 2%–4% increase in moderate to heavy rain in the postboost compared to the preboost period. The adjustment of the preboost data is consistent with the work of *DeMoss and Bowman* [2007] who found that there is a strong negative bias of TMI rain over the entire tropics compared to the preboost gauge data. For PR, the postboost data have significantly less (6%–8%) light rain, 2%–4% less moderate to light rain, and about 7%–10% less heavy rain, which is consistent with the boost effects on PR data reported by *Shimizu et al.* [2009] and by *Short and Nakamura* [2010].

[7] Probability distribution functions (pdf) for rainfall and joint pdfs (jpdfs) of cloud top brightness temperature (T_b) and echo top height (H_{ET}) are constructed to characterize the rain-cloud system as a function of percentile ranked rain rates. As a first step, we focus on changes in rainfall characteristics sampled from daily data for all 12 years of TRMM data over the tropical (25°S–25°N) oceans, as a function of tropical mean SST. Seasonality and regional changes in rainfall characteristics will be reported in a separate paper (K.-M. Lau and H.-T. Wu, manuscript in preparation, 2011). In this study, we only examine changes in tropical rainfall over oceans associated with changes in mean SST as a first step to understand climate change. More future work to investigate the changes of precipitation over land is required to get a complete picture of the possible hydrological response associated with warmer climate.

3. Climatological Rainfall pdf

[8] The climatological (1998–2009) rainfall pdf for the tropical (25°S–25°N) oceans based on TMI and PR are constructed for the frequency of occurrence (FOC) (Figure 1a) and the yearly accumulated rain amount (Figure 1b) as a function of rain rate. Note that the associated rain rate of a particular rain occurrence shown in Figure 1 is not an instantaneous measurement of such rain event, but rather an unconditional mean of different rain rates (including 0) within the 0.5° grid box and a day period. The frequent occurrence of the lightest rain shown in Figure 1a is most likely the average of light rain and no rain pixels, considering the low sensitivity of TMI and PR in detecting the actual drizzle.

[9] Both TMI and PR indicate that over the tropical oceans, lighter rain events dominate the rain occurrence, and moderate rain events account for the major rain amount contribution. Comparing to PR, TMI underestimates the FOC

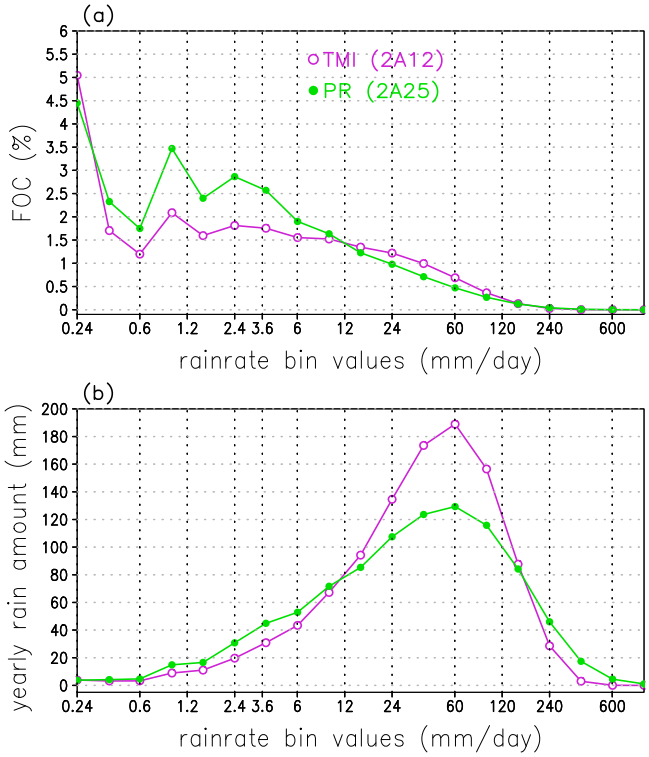

Figure 1. Probability distribution functions (pdf) of tropical oceanic rain: (a) frequency of occurrence (FOC) and (b) annual rain amount as a function of rain rate based on TRMM Microwave Imager (TMI) and Precipitation Radar (PR) data.

of light rain events (0.3–10 mm d^{-1}) but overestimates the FOC of moderate to heavy rain events (12–150 mm d^{-1}). At the extreme ends of rain spectrum, TMI estimates higher FOC of the lightest (<0.25 mm d^{-1}) rain, while PR estimates higher FOC for the most intense (>155 mm d^{-1}) rain events. Such relative bias in FOC leads to a large underestimation of PR rain amount, compared to TMI, in the intermediate range, and slight overestimation in rainfall amount for light rain and heavy rain (Figure 1b). These amount to a 9% underestimation of total accumulated annual rain for PR (960 mm yr^{-1}) relative to TMI (1060 mm yr^{-1}). Several factors may contribute to the disagreement between the TMI and PR rain retrievals, including the different physical principles, swaths and pixel sizes, sensitivities on the rain–no rain detection between TMI and PR measurements, and the different ambiguity and biases of their algorithms. The estimated 5.9% decrease in the PR rain due to boost effects shown by *Shimizu et al.* [2009] may also contribute to this disagreement. The differences between TMI- and PR-derived tropical annual total rain amounts and between their pdf (Figure 1) found in this study are consistent with results in previous studies [*Kummerow et al.*, 2000; *Masunaga et al.*, 2002; *Lin and Hou*, 2008] using shorter data periods, different data versions, and different spatial-temporal resolutions.

[10] On the basis of the individual rain pdf, rain categories are defined for TMI and PR. Following *Lau and Wu* [2007], light rain is defined as rainfall with the lowest 5% accumulated rain amount (B5), heavy rain as that at the top 10% (T10), and rainfall within the interquartile range as the intermediate rain (I25). For TMI, the threshold rain rates for B5, I25, and T10 are 3.6, 21.6–98.4, and 156 mm d^{-1}, respectively. For PR, the corresponding thresholds are 2.4, 14.4–108, and 201.6 mm d^{-1}. With the above definitions, we find that for the tropics as a whole, the TMI and PR estimates are consistent in that light rain (B5) contributes to more than 50% of the rainy days, while by definition they contribute only 5% of the rain amount. On the other hand, the occurrence of heavy rain events (T10) is very rare, i.e., less than 1%, though they contribute twice the rain amount of B5 rain.

[11] The spatial distributions of the climatological annual FOC, defined as averaged percentage of rainy days in a year, are constructed from the subset of the rainfall data binned according to the above-described ranked rain rates. The geographic distributions are qualitatively similar between TMI and PR. For economy of space, we show in Figure 2 only results using TMI data, with any distinct differences between TMI and PR patterns noted in the discussion. Light rain B5 (Figure 2a) is found over large expanses of tropical and subtropical oceans, with high FOC (15%–25%) over the Intertropical Convergence Zone (ITCZ) but weak spatial gradients suggesting weak thermodynamic control by the warm pool, and by subtropical storm tracks. Intermediate rain I25 (Figure 2b) occurs mostly over the warm pool regions, with a maximum FOC of approximately 13% around tropical central Pacific (130°W–140°W), as well as local maxima (FOC ~ 7%–10%) over the tropical western Pacific, the South Pacific Convergence Zone (SPCZ), the eastern Indian Ocean, and the Atlantic ITCZ. Note that the local rainfall maximum over the tropical central Pacific based on TMI data is of smaller magnitude and less distinct in the PR I25 pattern. This regional disagreement between TMI and PR data is also noted by *Ikai and Nakamura* [2003]. They indicate such disagreement is most likely due to the difference between the bright band height from PR and the specified freezing level in the TMI algorithm. In general, the I25 pattern shows the clear imprint of the warm pool (see contours of SST in Figure 2d), suggesting strong thermodynamic control of the underlying warm pool. For heavy rain, T10 (Figure 2c) exhibits the largest spatial gradient of the rain categories, with maximum occurrences (FOC > 0.5%) over the core convective regions of the Pacific ITCZ, the SPCZ, the Bay of Bengal, and the oceanic regions in the vicinity of the Philippines. The tight spatial gradient for T10 is consistent with the close connection between organized deep convection and large-scale dynamics, i.e., low-level moisture convergence, in addition to the control of the warm pool. The spatial pattern of the FOC of total rain (contributed by all rain types) (Figure 2d) shows that rain falls most frequently over the ITCZ and SPCZ regions, and least frequently off the west coast of the continents in the subtropics, in coincidence with the region of large scale subsidence and widespread coastal stratiform clouds. Note that TRMM rain retrievals might not be sensitive enough to observe very light drizzle, and as a result, the feature of the southeast Pacific stratus deck is absent in Figure 2d. However, this feature is revealed in TRMM cloud liquid water (CLW) data (analyzed but not shown in this study) as well as the CLW analysis of *Xu et al.* [2005]. We note that even in regions of deep convection, rainfall is not

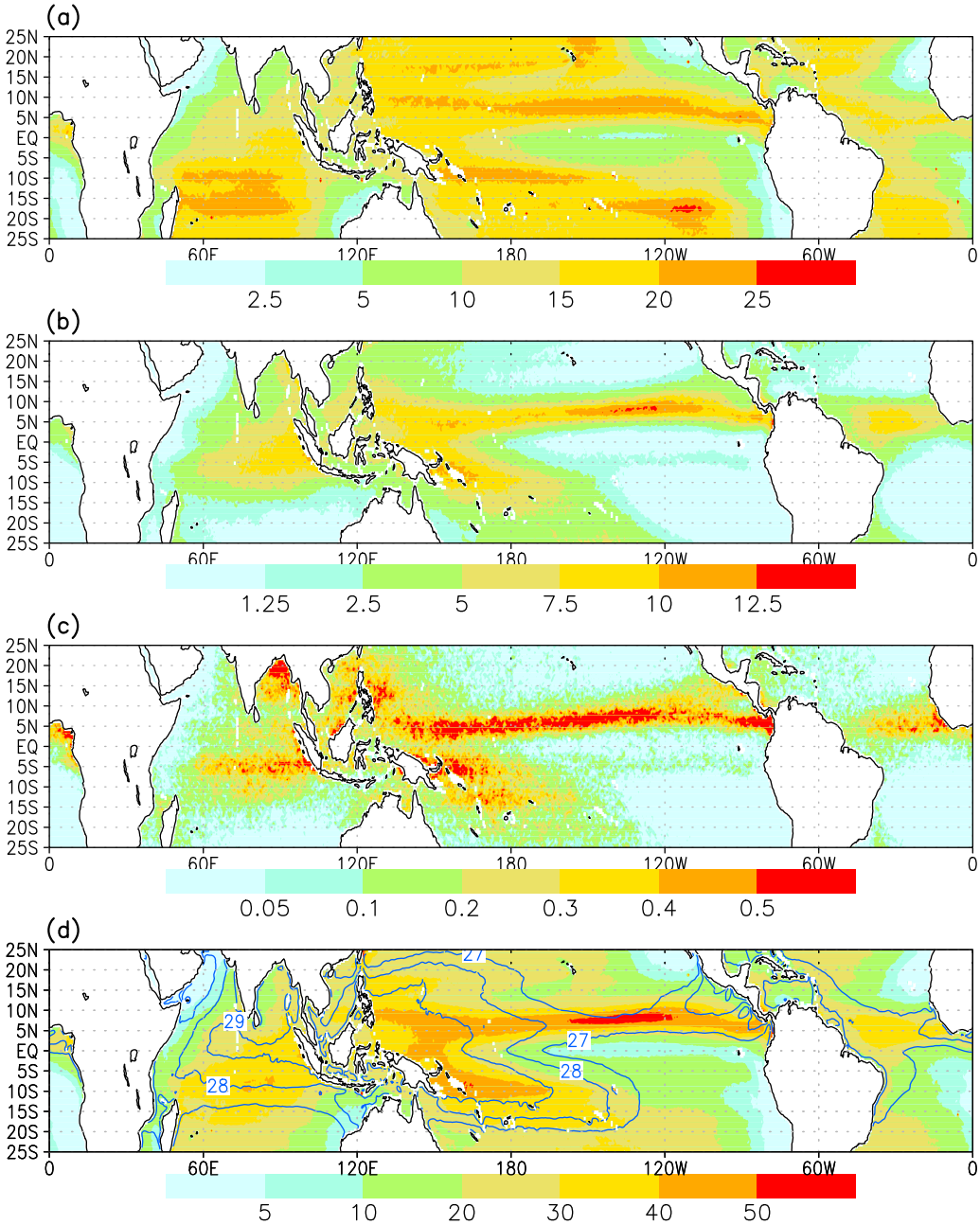

Figure 2. Geographic distribution of rain occurrence of each rain category based on TMI data for (a) B5, (b) I25, (c) T10, and (d) total rain in percentage of a year (365 days). Superimposed on Figure 2d, the shaded total rain pattern is sea surface temperature in contour lines of 27°C, 28°C, and 29°C. Note different color scales are used in each panel.

all due to heavy rain types, but rather consists of a mix of light, intermediate, and heavy rains. This is consistent with observations that convective organization in the tropics such as the ITCZ and Madden-Julian Oscillations (MJO) involves all rain types [*Lau and Wu*, 2010].

4. Joint pdfs of Cloud and Rain Distribution

[12] To identify the cloud and rain characteristics associated with the different rain types, we construct two-dimensional jpdfs from daily cloud top temperature (T_b), and echo top height (H_{ET}) over all tropical oceans (Figure 3), with the preboost rain rate adjusted on the basis of the procedure described in section 2. The H_{ET} is the maximum height of hydrometeors in the rain system, detectable by PR. A simple classification scheme can be derived on the basis of the climatological jpdfs (Figure 3a). On the basis of reference of the freezing point of 273 K for cloud top temperature (T_{b0}) and freezing and melting level at H_{ET0} = 5 km for the tropics, a region in the T_b-H_{ET} space which is significantly higher than T_{b0} and lower than the H_{ET0} (lower left quadrant of jpdfs in Figure 3) can be identified with low cloud and warm or liquid phase rain system. Similarly a region in T_b-H_{ET} space significant lower than

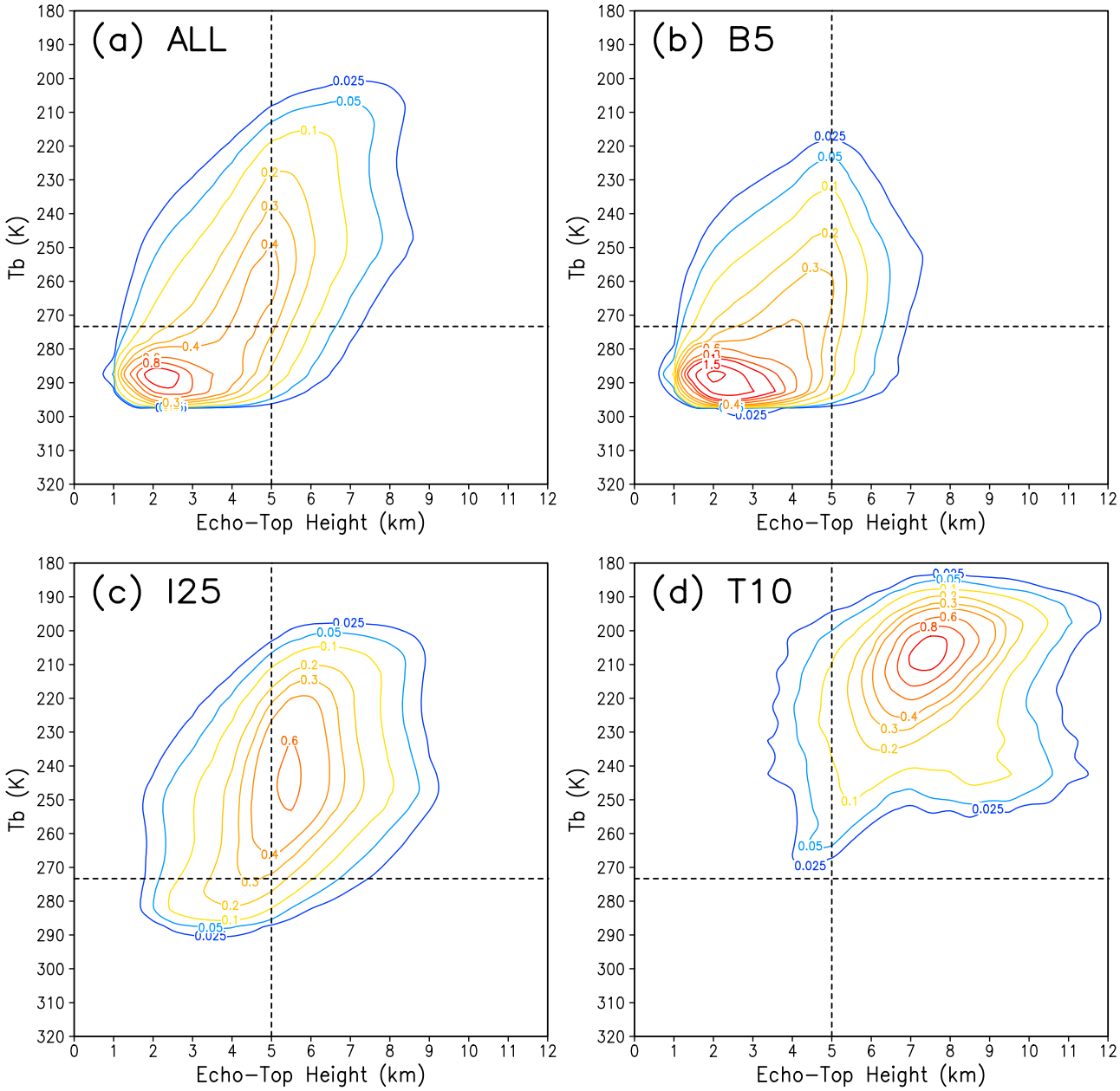

Figure 3. Joint probability distribution functions of TRMM PR echo top height and Visible and Infrared Scanner (VIRS) channel-4 brightness temperature (T_b) based on daily data for tropical oceanic (a) total (all rain types), (b) B5, (c) I25, and (d) T10 rains. Contour levels are 0.025, 0.05, 0.1, 0.2, 0.3, 0.4, 0.6, 0.8, 1.0, 1.5, 2, 2.5, 3, 3.5, and 4, in units of % km^{-1} K^{-1} of 12 year (1998–2009) averaged total counts of each rain category.

T_{b0} and higher than H_{ET0} reflects a cold cloud top, deep convective rain system. A large population in the region (4 km < H_{ET} < 6 km, 220 K < T_b < 300 K) can be identified as mixed phase rain-cloud system. *Masunaga and Kummerow* [2006] and *Matsui et al.* [2009] reported similar classifications and further subdivided the mixed-phase regime into congestus (Tb > 245 K, 4 km < H_{ET} < 6 km) and congestus with overlapping cirrus (Tb < 245 K, 4 km < H_{ET} < 6 km). For the purpose of this work, such subdivision is not necessary. Figures 3b, 3c, and 3d show the jpdfs constructed separately for B5, I25, and T10 rain, respectively. The jpdfs for B5 show a pronounced local maximum at (290 K, 2 km), indicating a large population of low-level, warm, light rain over the tropics. The intermediate rain, I25, is associated primarily with mixed-phase, middle to high cloud systems, as evident in the broad distribution of T_b and H_{ET} around the pronounced local maximum near (230–260 K, 4–6 km). The T10 rain occupies a region (190–220 K, 6–9 km) that is predominantly associated with deep convection and ice phase precipitation. Note that several rain and cloud types may be averaged together because of the use of the common 0.5° grid box average instead of the original instantaneous value. As a result, Figure 3 shows a smoother histogram of tropical rain systems compared to that shown by *Masunaga*

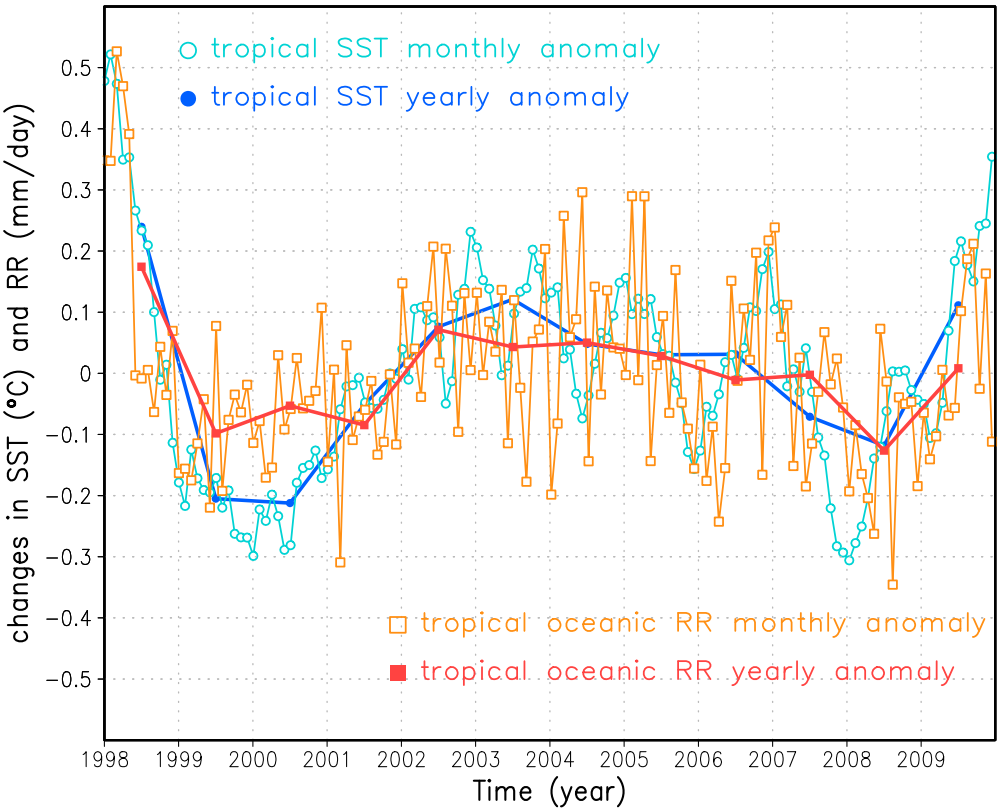

Figure 4. Time series of tropical annual and monthly mean SST and tropical mean oceanic rainfall (RR) anomalies from the 1998–2009 climatology.

and Kummerow [2006]. Furthermore, while we use simplified terms of mixed-phase and ice phase precipitation to provide a general picture of cloud characteristics associated with different rain systems, the actual cloud structure can be much more complex. For example, rain systems that belong within 4 km < H_{ET} < 6 km can also contain a fair amount of fluffy snowflakes undetectable by the PR. On the other hand, rain systems with H_{ET} > 7 km certainly contain developed ice phase precipitation but at the same time may also include supercooled droplets, and hence may possess mixed-phase characteristics.

5. Changes in Rainfall Characteristics With SST

[13] Figure 4 shows the time series of monthly anomalies (seasonal cycles removed) and annual anomalies of tropical mean SST and tropical mean oceanic TMI rainfall during the TRMM data period (1998–2009). There is no discernable trend in total rainfall during the period. While the tropical mean SST anomalies are dominated by interannual variability with relatively small monthly perturbations, the rainfall anomaly undergoes large intermonthly and interannual fluctuations. As indicated in Figure 4, the magnitude of the tropical annual mean SST ($\overline{SST}$) fluctuations (<0.2°C) is much smaller than regional signals such as ENSO (~1°C–2°C). The SST and rainfall tropical annual means (solid lines) suggest a high degree of coherence in the background low-frequency variations. From Table 1, the correlation of SST and rainfall is 0.85 in the annual tropical mean and 0.52 in the monthly tropical mean, both significant at above the 99% level. However, with the low-frequency signal removed, the monthly correlation drops to 0.31, indicating that the primary source of the significant covariability between SST and rainfall is in the tropical annual mean fields. For PR (see Table 1), the correlations of monthly and annual tropical mean with SST are lower compared to TMI, possibly because of the larger sampling errors stemming from the narrower swath of PR. Henceforth, we use $\overline{SST}$ as the control variable for examining the possible changes in rainfall characteristics. However, we recognize that because of the ways the warm and cold regions in the oceans are set up by the large-scale ocean-atmosphere circulation, even a tropical mean SST signal will have spatial structures. Changes in rainfall characteristics are likely a function of not only the overall SST, but also the gradient of SST. It is possible that

Table 1. Linear Correlation Between SST, TMI, and PR Rain Rates Over Tropical (25°S–25°N) Oceans for the 1998–2009 Period[a]

Variables	Monthly Anomalies	Annual Mean	Monthly Anomalies (Annual Mean Removed)
⟨SST, TMI⟩	**0.52**[b]	**0.85**[b]	**0.31**[b]
⟨SST, PR⟩	**0.20**[b]	**0.68**	0.05
⟨TMI, PR⟩	**0.78**[b]	**0.65**	**0.83**[b]

[a]Values exceeding 95% significance level are highlighted in bold. SST, sea surface temperature; TMI, TRMM Microwave Imager; PR, Precipitation Radar.
[b]Greater than 99% significance.

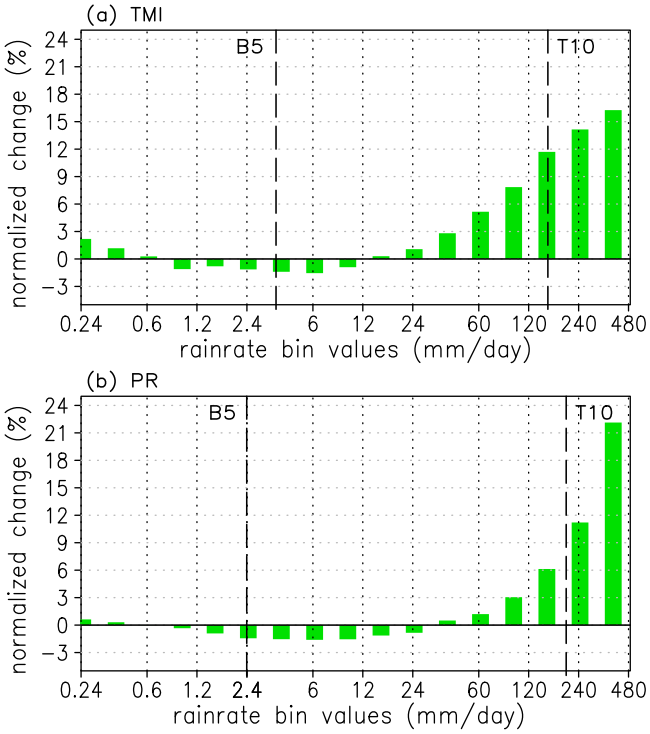

Figure 5. Composite of normalized change of averaged annual rain amount from six cold years (1999, 2000, 2001, 2005, 2007, and 2008) to six warm years (1998, 2002, 2003, 2004, 2006, and 2009) as a function of rain rate based on (a) TMI and (b) PR data.

both types of warming or cooling, i.e., due to SST gradient and due to overall warming, may be at work over the entire tropics during the data period. The use of tropical mean SST in our paper is a crude measure of both effects, and as a convenient reference to SST change. We make no attempt to separate the two effects in this work.

[14] To examine the impacts of $\overline{SST}$ on daily rainfall characteristics, we first divide the 12 years of TRMM data into two halves according to the magnitude of $\overline{SST}$ anomaly. We then construct the composite rainfall pdf for the two halves, and compute the difference of the composite pdf between the warm and cold halves from both PR and TMI. The TMI data (Figure 5a) indicate that warmer SST years are associated with a pronounced increase in moderate to heavy to very heavy rain (rain rate > 60 mm d^{-1}) amount, a mild reduction in light to moderate light rain (rain rate ~ 1–12 mm d^{-1}) amount, and a small increase (<3%) of extremely light (drizzle) rain (rain rate < 0.6 mm d^{-1}) amount. For T10 rain, the increase is more than 12%–15%. For PR data (Figure 5b) we find qualitatively similar features consistent with those of TMI. Compared to TMI, PR captures more extremely heavy rain events (see also Figure 1b), with increase in T10 rain amount exceeding 20% from cold to warm years. The increase in drizzle rain in PR analysis is not as obvious as that shown in TMI, which may be due to the limitation of PR retrievals of very light rain events. With the years of strong warm (1998 and 2003) and strong cold events (2000 and 1999) removed, the pdf difference pattern (not shown) remains similar, albeit the signals are weaker.

[15] The increase in heavy and very heavy rain with higher $\overline{SST}$ is associated mostly with an overall shift to rain

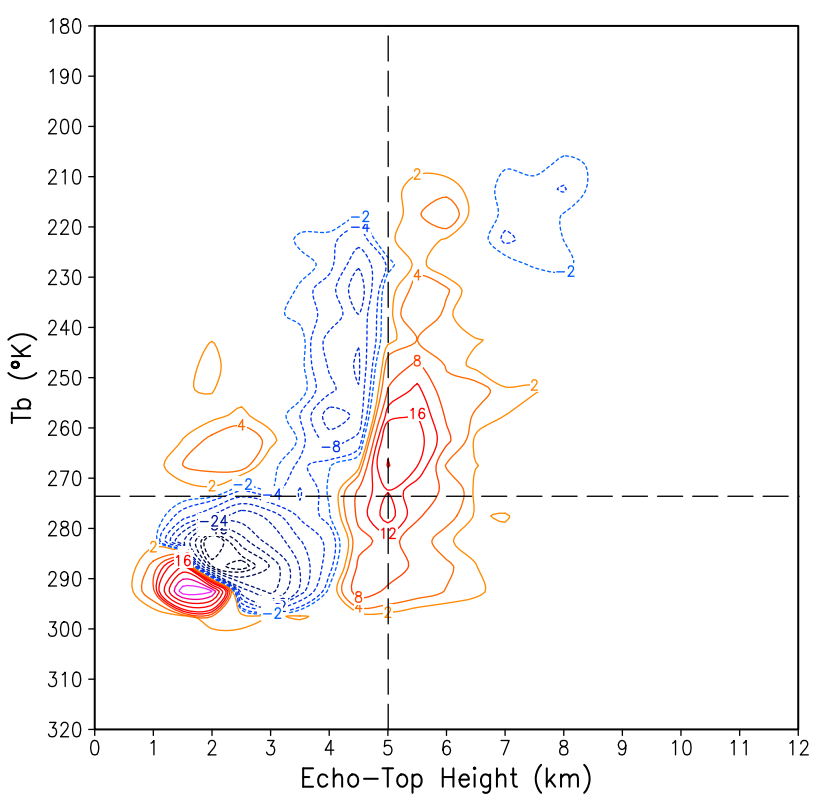

Figure 6. Same as in Figure 3, except for the composite differences between the six warm and the six cold years within the 1998–2009 period.

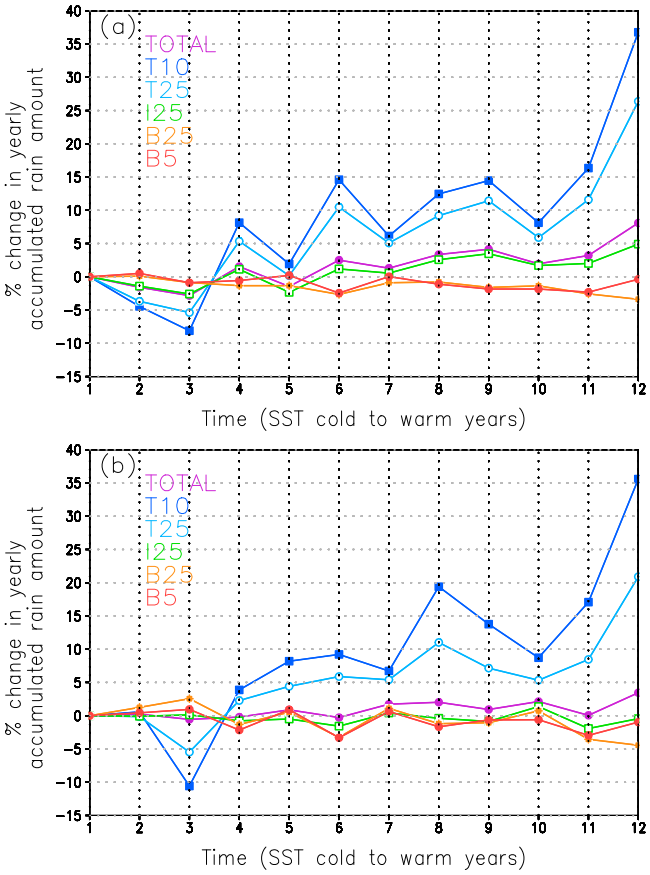

Figure 7. Changes of annual rain amount for five different rain categories, B5, B25 (bottom 25%), I25, T25 (top 25%), T10, and total (all rain types) based on (a) TMI and (b) PR as a function of tropical mean SST, arranged from the coldest to the warmest SST year (in the order of 2000, 1999, 2008, 2007, 2001, 2005, 2006, 2004, 2002, 2009, 2003, and 1998).

systems with increased H_{ET}, implying deeper rain layer for all cloud-rain types, as evidenced in the dipole-like structure in the warm minus cold difference jpdfs (Figure 6). The large reduction in light rain (B5, lower left quadrant) is primarily associated with a decrease in population of low-cloud, liquid phase rain systems. There appears to be a pronounced increase in the amount of light rain from very low (H_{ET} ~ 1–2 km) and warm (T_b ~ 290–300 K) cloud, probably associated with a warmer marine boundary layer over the subtropics with higher $\overline{SST}$ (see B5 rain distribution in Figure 2a). A weak positive anomaly is found in the region T_b ~260–270 K, and H_{ET} ~ 2 km, well below the freezing level, indicating a slight increase in liquid phase rain, with middle clouds. A weak negative anomaly is also found in the deep convective region (H_{ET} > 7 km, 210 K < T_b < 230 K). As we find from ongoing work (K.-M. Lau and H.-T. Wu, manuscript in preparation, 2011), these weak anomalies are related to the residual effects from ENSO, arising from influence of the rising and sinking branches of the Walker circulation, in conjunction with the warming of the central and eastern equatorial Pacific.

[16] To further illustrate the changes in rainfall characteristics as a function of $\overline{SST}$, Figure 7 shows the variation of yearly accumulated rain amount for five rain categories, B5, B25 (bottom 25%), I25, T25 (top 25%), T10, and total (all rain types), with years arranged in ascending order from low to high $\overline{SST}$ and relabeled year 1 (coldest) through year 12 (warmest). The percentage changes in accumulated rain amount have been normalized to year 1. Both TMI (Figure 7a) and PR (Figure 7b) indicate a slight downward slope for B5 and B25 rain, a neutral to slightly upward slope for I25 and for total rain amount, and a clear upward slope for T25 and T10 rain. The large positive slope of T10 rain as a function of increasing tropical mean SST suggests that among all rain types, extreme (heavy) rain is most sensitive to the changes in $\overline{SST}$ and $\overline{SST}$-induced circulation feedbacks.

[17] The sensitivity of the rate of change in rain amount of different rain types to the change in $\overline{SST}$ is estimated by separating the rain amount into 11 categories based on the percentile contribution (with 10% interval for the first nine bins, and 5% interval for the last two bins) of the corresponding rain amount as defined in section 3. The percentage change of rain amount of different rain types (bins) to SST changes (dP/P/dSST) or rainfall sensitivity is then computed on the basis of linear regression of the slope of the changes as a function of SST (see Figure 7) for each rain bin for both TMI and PR. Figure 8 shows the variation of rainfall sensitivity for TMI and PR. Both show positive rainfall sensitivity for moderate to heavy to very heavy rain (the last 6 bins, or T50), and negative sensitivity for light to moderate rain (the first 3 bins, or B30). All calculated rainfall sensitivities are significant to the 95% confidence levels (with corresponding ±1.96 standard deviation marked by vertical bar), except for the transition zone around the 20th to 40th percentile rain rate (bins 3 and 4) for TMI and 30th to 60th percentile (bins 4–6) for PR. While TMI and PR data show some quantitative differences in rainfall sensitivity and in the thresholds of the transition zone, both show similar pattern, with very heavy rain events (last two bins) showing most sensitivity to the SST change. The rainfall sensitivity for the most extreme rain events (T5) is approximately +80%–90% K^{-1} for both TMI and PR analyses. Both TMI and PR show negative sensitivity for light to moderate rain (<30th percentile), most likely reflecting the effects of suppressed rain because of widespread subsiding motion associated with any significant increase in organized deep convection (heavy rain events) in a warmer tropical ocean. The overall rainfall sensitivity for total rain is estimated to be +18% K^{-1} ± 3% K^{-1} for TMI and +6% K^{-1} ± 1.7% K^{-1} for PR.

[18] The overall TMI rainfall sensitivity is comparable to the +19.3% K^{-1} estimated for tropical oceanic rain in previous studies using GPCP monthly data [*Adler et al.*, 2008; *Allan et al.*, 2010]. On the other hand, the PR rainfall sensitivity is comparable to the 9.1% K^{-1} relation of water vapor and SST analyzed by *Wentz et al.* [2007] using SSM/I monthly data. The discrepancy between the TMI and PR rainfall sensitivity is not surprising because the algorithms of TMI and PR rain retrievals are based on different physical principles. However, it is difficult to quantify the exact source of the discrepancy. The cause for the lower rainfall sensitivity for PR total rain is probably the same as that

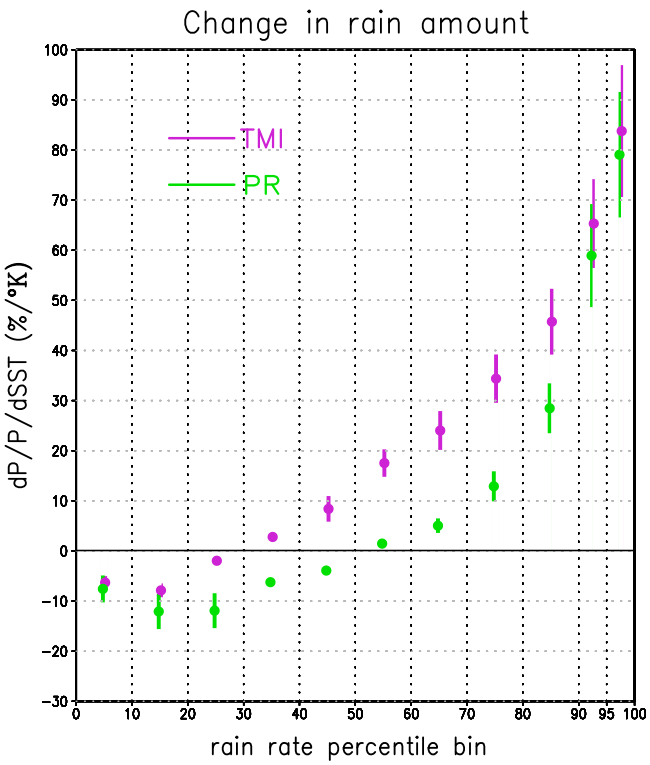

Figure 8. Changes in annual rain amount per degree K sea surface temperature rise calculated from linear regressions by rain category (classified by contributed rain amount percentile, defined in section 3) from TMI and PR data. Linear fits with significant (>95%) confidence levels are noted with their corresponding ±1.96 standard deviation marked by vertical bars.

responsible for the relative underestimate of moderate to heavy rain accumulation in the PR rain pdf (see discussion for Figure 1b).

6. Conclusions

[19] Using TRMM daily rainfall observations, we have examined the climatology and changes of tropical oceanic rainfall characteristics. Surface rainfall estimates from two different sensors, i.e., TMI and PR, are analyzed and compared. Compared with TMI, PR substantially underestimates intermediate rain, but overestimates very light and very heavy rains, with a 9% underestimate in total tropical annual rain accumulation. Even with these systematic biases, both PR and TMI show consistent qualitative results regarding the climatology in rainfall characteristics, and their changes as a function of sea surface temperature. Light rain is mostly associated with low clouds and liquid phase rain over large span of the tropical and subtropical oceans. Intermediate rain is associated with mixed-phase rain and middle to high clouds in the warm pool regions of Indian Ocean, tropical Pacific and tropical Atlantic Oceans. Heavy rain is associated with ice phase deep convection in the cores of the ITCZ, SPCZ and summer monsoon regions. Both TMI and PR show a significant shift in rainfall pdf as a function of tropical mean SST, reflecting a large percentage increase in very heavy rain, coupled to a reduction in light to moderate rain over a warmer ocean.

[20] This study also suggests that even though a chronological trend in total rainfall is absent in the relatively short-term (12 years) TRMM data record, useful information regarding possible changes in rainfall characteristics with respect to SST may be inferred from TRMM data. We find that extreme rain events are most sensitive to the changes in tropical mean SST. Both TMI and PR show that the amount of extreme heavy (95th percentile) rain could increase 80%–90% per degree SST rise, much higher than the 7% increase of water vapor per degree SST expected from the Clausius-Clapeyron equation for global water balance closure. This is because extreme heavy rain is not a close system in itself, but rather one that is associated with ice phase processes with strong convective dynamic feedback. In addition, we find a negative sensitivity of light and moderate rain (<30th to 40th percentile) to SST, reflecting a possible adjustment of the populations of tropical rain and convective systems to overall warming or cooling of the tropics.

[21] Finally, it should be stressed that the statistics for rain characteristics are likely to be highly sensitive to the data window, and retrieval algorithms. In particular, for studies using preboost and postboost data, quantitative results may be sensitive to the systematic bias introduced by the orbit boost, and adjustment procedures. It is therefore reassuring that both PR and TMI data show very comparable higher sensitivity for extreme events (90th percentile or higher), and that both pdfs show similar qualitative distribution shift as a function of SST. The present results indicate that regardless of the retrieval algorithms used, and in spite differences in total rain amounts and trend estimates over the tropics, both PR and TMI could capture important common changes in physical processes related to SST change. Because of the short record of the TRMM data, the SST sensitivities estimated here include both effects of interannual, i.e., ENSO, as well as decadal-scale variability. Moreover, the low capability of TRMM in observing drizzle or isolated light rain and the smoothing effect due to the use of 0.5° grid box average preclude the investigation of organization from subgrid scale rain system, such as the ratio of raining to nonraining pixels within each grid box, associated with mean tropical SST. The estimation of sensitivity of rainfall characteristics to surface temperature as a function of spatial and temporal scales and for longer periods will have to await the availability of long-term, high-quality, high-resolution data extending and merging the TRMM rainfall products with those from Global Precipitation Mission.

[22] **Acknowledgments.** This research is supported by the Precipitation Measurement Mission, NASA headquarters (Program Manager R. Kakar). The authors would like to thank three anonymous reviewers for providing constructive and critical comments on the paper.

References

Adler, R. F., G. Gu, J. Wang, G. J. Huffman, S. Curtis, and D. Bolvin (2008), Relationships between global precipitation and surface temperature on interannual and longer timescales (1979–2006), *J. Geophys. Res.*, *113*, D22104, doi:10.1029/2008JD010536.

Allan, R. P., and B. J. Soden (2008), Atmospheric warming and the amplification of precipitation extremes, *Science*, *321*, 1481–1484, doi:10.1126/science.1160787.

Allan, R. P., B. J. Soden, V. O. John, W. Ingram, and P. Good (2010), Current changes in tropical precipitation, *Environ. Res. Lett.*, *5*, 025205, doi:10.1088/1748-9326/5/2/025205.

Allen, M. R., and W. J. Ingram (2002), Constraints on future changes in climate and the hydrologic cycle, *Nature*, *419*, 224–232, doi:10.1038/nature01092.

DeMoss, J. D., and K. P. Bowman (2007), Changes in TRMM retrievals due to the orbit boost estimated from rain gauge data, *J. Atmos. Oceanic Technol.*, *24*, 1598–1607, doi:10.1175/JTECH2082.1.

Easterling, D. R., J. L. Evans, P. Y. Groisman, T. R. Karl, K. E. Kunkel, and P. Ambenje (2000), Observed variability and trends in extreme climate events: A brief review, *Bull. Am. Meteorol. Soc.*, *81*, 417–425, doi:10.1175/1520-0477(2000)081<0417:OVATIE>2.3.CO;2.

Gu, G., R. F. Adler, G. Huffman, and S. Curtis (2007), Tropical rainfall variability on interannual-to-interdecadal and longer time scales derived from the GPCP monthly product, *J. Clim.*, *20*, 4033–4046, doi:10.1175/JCLI4227.1.

Held, I. M., and B. J. Soden (2006), Robust responses of the hydrological cycle to global warming, *J. Clim.*, *19*, 5686–5699, doi:10.1175/JCLI3990.1.

Ikai, J., and K. Nakamura (2003), Comparison of rain rates over the ocean derived from TRMM Microwave Imager and Precipitation Radar, *J. Atmos. Oceanic Technol.*, *20*, 1709–1726, doi:10.1175/1520-0426(2003)020<1709:CORROT>2.0.CO;2.

Intergovernmental Panel on Climate Change (2007), *Climate Change 2007: The Physical Science Basis. Contribution of Working Group I to the Fourth Assessment Report of the Intergovernmental Panel on Climate Change*, edited by S. Solomon et al., Cambridge Univ. Press, Cambridge, U. K.

Kummerow, C., W. Barnes, T. Kozu, J. Shiue, and J. Simpson (1998), The tropical rainfall measuring mission (TRMM) sensor package, *J. Atmos. Oceanic Technol.*, *15*, 809–817, doi:10.1175/1520-0426(1998)015<0809:TTRMMT>2.0.CO;2.

Kummerow, C., et al. (2000), The status of the Tropical Rainfall Measuring Mission (TRMM) after two years in orbit, *J. Appl. Meteorol.*, *39*, 1965–1982, doi:10.1175/1520-0450(2001)040<1965:TSOTTR>2.0.CO;2.

Lau, K. M., and H. T. Wu (2003), Warm rain processes over tropical oceans and climate implications, *Geophys. Res. Lett.*, *30*(24), 2290, doi:10.1029/2003GL018567.

Lau, K. M., and H. T. Wu (2007), Detecting trends in tropical rainfall characteristics, 1979–2003, *Int. J. Climatol.*, *27*, 979–988, doi:10.1002/joc.1454.

Lau, K. M., and H. T. Wu (2010), Characteristics of precipitation, cloud, and latent heating associated with the Madden-Julian Oscillation, *J. Clim.*, *23*(3), 504–518, doi:10.1175/2009JCLI2920.1.

Lau, K. M., Y. P. Zhou, and H. T. Wu (2008), Have tropical cyclones been feeding more extreme rainfall?, *J. Geophys. Res.*, *113*, D23113, doi:10.1029/2008JD009963.

Lin, X., and A. Y. Hou (2008), Evaluation of coincident passive microwave rainfall estimates using TRMM PR and ground measurements as references, *J. Appl. Meteorol. Climatol.*, *47*, 3170–3187, doi:10.1175/2008JAMC1893.1.

Lin, X., L. D. Fowler, and D. A. Randall (2002), Flying the TRMM satellite in a general circulation model, *J. Geophys. Res.*, *107*(D16), 4281, doi:10.1029/2001JD000619.

Masunaga, H., and C. D. Kummerow (2006), Observations of tropical precipitating clouds ranging from shallow to deep convective systems, *Geophys. Res. Lett.*, *33*, L16805, doi:10.1029/2006GL026547.

Masunaga, H., T. Iguchi, R. Oki, and M. Kachi (2002), Comparison of rainfall products derived from TRMM Microwave Imager and Precipitation Radar, *J. Appl. Meteorol.*, *41*, 849–862, doi:10.1175/1520-0450(2002)041<0849:CORpdf>2.0.CO;2.

Matsui, T., X. Zeng, W.-K. Tao, H. Masunaga, W. Olson, and S. Lang (2009), Evaluation of long-term cloud-resolving model simulations using satellite radiance observations and multi-frequency satellite simulators, *J. Atmos. Oceanic Technol.*, *26*, 1261–1274, doi:10.1175/2008JTECHA1168.1.

Rayner, N. A., D. Parker, E. Horton, C. Folland, L. Alexander, D. Rowell, E. Kent, and A. Kaplan (2003), Globally complete analyses of sea surface temperature, sea ice and night marine air temperature, 1871–2000, *J. Geophys. Res.*, *108*(D14), 4407, doi:10.1029/2002JD002670.

Shepherd, J. M., A. Grundstein, and T. L. Mote (2007), Quantifying the contribution of tropical cyclones to extreme rainfall along the coastal southeastern United States, *Geophys. Res. Lett.*, *34*, L23810, doi:10.1029/2007GL031694.

Shimizu, S., R. Oki, T. Tagawa, T. Iguchi, and M. Hirose (2009), Evaluation of the effects of the orbit boost of the TRMM satellite on PR rain estimates, *J. Meteorol. Soc. Jpn.*, *87A*, 83–92, doi:10.2151/jmsj.87A.83.

Short, D. A., and K. Nakamura (2010), Effect of TRMM orbit boost on radar reflectivity distributions, *J. Atmos. Oceanic Technol.*, *27*, 1247–1254, doi:10.1175/2010JTECHA1426.1.

Trenberth, K. E., A. Dai, R. M. Rasmussen, and D. B. Parsons (2003), The changing character of precipitation, *Bull. Am. Meteorol. Soc.*, *84*, 1205–1217, doi:10.1175/BAMS-84-9-1205.

Wentz, F. J., L. Ricciardulli, K. Hilburn, and C. Mears (2007), How much more rain will global warming bring?, *Science*, *317*, 233–235, doi:10.1126/science.1140746.

Xu, H., S.-P. Xie, and Y. Wang (2005), Subseasonal variability of the southeast Pacific stratus cloud deck, *J. Clim.*, *18*, 131–142, doi:10.1175/JCLI3250.1.

K.-M. Lau, Laboratory for Atmospheres, Code 613, NASA Goddard Space Flight Center, Bldg. 33, Rm. C121, Greenbelt, MD 20771, USA. (william.k.lau@nasa.gov)

H.-T. Wu, Science Systems and Applications, Inc., 10210 Greenbelt Rd., No. 600, Lanham, MD 20706, USA.